Soil Dynamics and Earthquake Engineering 124 (2019) 1–15

Contents lists available at ScienceDirect

Soil Dynamics and Earthquake Engineering

journal homepage: www.elsevier.com/locate/soildyn

Effect of layered liquefiable deposits on the seismic response of soil-foundations-structure systems

Guillermo A. López Jiménez[a], Daniel Dias[b,c,*], Orianne Jenck[a]

[a] Univ. Grenoble Alpes, CNRS, Grenoble INP**, 3SR, F-38000, Grenoble, France
[b] Hefei University of Technology, School of Automotive and Transportation Engineering, Hefei, China
[c] Antea Group, Antony, France

ARTICLE INFO

Keywords:
Liquefaction
Soil constitutive models
Pile foundation
Numerical modelling
Dynamic analysis

ABSTRACT

The soil liquefaction is a major cause of damage in structures during earthquakes. This damage varies from small settlements to complete failure due to the loss of bearing capacity. To deal with these problems, piled foundations have been utilized in the presence of liquefiable soils in seismic zones. More recently, rigid inclusion foundations have been also considered. A fundamental approach to study the soil-foundation-structure interaction requires the determination of the influence of the kinematic and inertial effects in the system. In order to investigate the effects of this interaction, numerical models with a 3-storey reinforced concrete building founded on pile systems (soil-pile-structure) and rigid inclusion systems (soil-inclusion-platform-structure) were analyzed. Finite difference numerical models were developed using Flac 3D. The SANISAND constitutive model was utilized to represent the behavior of the liquefiable soil layer. This model predicts with accuracy the soil response for various soil densities, stress levels and loading conditions. The linear elastic perfectly plastic constitutive model with a Mohr-Coulomb failure criterion was used to represent the behavior of the non-liquefiable soil layers. Different relative density values of the sand layer were considered. Two earthquake signals were used to study the influence of the frequency of the systems excitation. For each case, the spectrum response, shear forces and rocking of foundations were obtained. Maximum shear strains and excess pore pressures were presented at different depths. The efforts and displacements in the rigid elements (piles or rigid inclusions) were also compared for the different systems. The results show that the relative density, the pile length and the frequency of the input motion greatly influence the response of the reinforced systems.

1. Introduction

Liquefaction is one of the significant and complex issues in geotechnical engineering because it has been reported as the main cause of damage and failure in buildings and other structures under earthquakes (Niiagata 1964, San Fernando 1971, Loma Prieta 1989, Kobe 1995). The liquefaction takes place due to the accumulation of pore pressure in loose saturated sand deposits under dynamic loading, which in turns produce an important reduction in the strength of the underlying soils. The loss of bearing capacity and the foundation settlements are the consequences of this soil strength reduction. To deal with these problems, piles foundations supporting structures are often used in seismically zones. More recently, rigid inclusion system has also been utilized. This method is similar to the pile foundation system; however, in this case the rigid elements are separated from the structure with the use of an earth platform (Fig. 1). The arching effect in the platform, caused by shearing mechanism due to differential settlements of soil and piles, allows a transfer of the load to the rigid inclusions. The remaining loads are transmitted to the underlying soil. The earth platform constitutes a zone of energy dissipation for seismic loading. The response of these foundation systems in the presence of liquefiable soil considers simultaneously, i) the dynamic loading acting in the rigid elements (piles/inclusions) due to the surrounding soil and the presence of the structure; ii) the shear strength reduction and the degradation of the soil stiffness due to the soil nonlinearities and the generation of pore pressure [1].

The behavior of pile foundations during earthquakes is often dictated by the soil-pile interaction, the response of the soil and the characteristics of the earthquake. Some authors have investigated the soil-pile-structure interaction using experimental test, with centrifuge tests: Abdoun et al. [2], Abdoun and Dobry [3], González et al. [4], Ramirez et al. [5] and Su and Li [6]; or with shaking table tests: Gao

* Corresponding author. Hefei University of Technology, School of Automotive and Transportation Engineering, Hefei, China.
E-mail addresses: alfonso.lopez@3sr-grenoble.fr (G.A. López Jiménez), daniel.dias@anteagroup.com (D. Dias), orianne.jenck@3sr-grenoble.fr (O. Jenck).

https://doi.org/10.1016/j.soildyn.2019.05.026
Received 14 December 2018; Accepted 15 May 2019
Available online 28 May 2019
0267-7261/

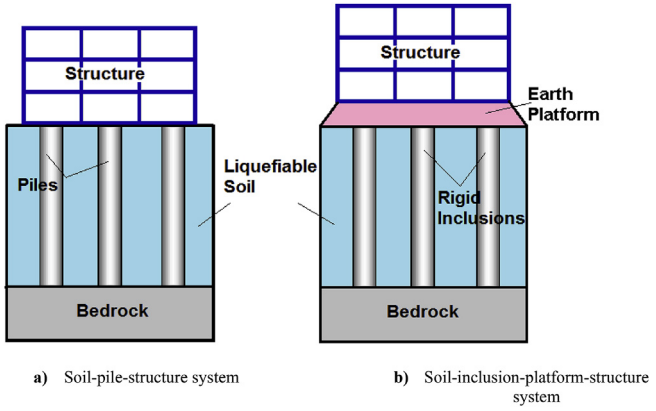

Fig. 1. Vertical reinforcement systems.

et al. [7], Haeri et al. [8] Tamura and Tokimatsu [9], Tokimatsu et al. [10]. Other authors have developed simplified methods to study the soil-pile-structure interaction in liquefiable soils [11–13]. More recently, Janalizadeh and Zahmatkesh [14] presented a pseudo-static method for the analysis of piles in liquefiable soil under seismic loadings. First a free-field site response analysis was done using 3D numerical modeling. A dynamic analysis of the pile and structure was performed using the time history of the ground surface. Finally the 1D Winkler seismic pile analysis was developed. They concluded that the *p-y* curves with various degradation factors in liquefiable sand produce reasonably results compared to centrifuge tests.

Other authors have separately evaluated soil constitutive models and numerical approaches in simulating soil-pile-structure systems. For example, Maheshwari and Sarkar [15] developed a 3D model in a finite element code of a 4-storey portal frame structure supported by a group of 4 piles. A work-hardening plastic cap model was used for the behavior of the soil. The pore pressure generation due to liquefaction was incorporated by a two-constant volume change expression. They determined that the effects of nonlinearity and liquefaction of the soil-pile system increased as the intensity of the excitation increases. Rahmani and Pak [16] analyzed a three-dimensional soil-single pile-structure system in a liquefiable soil. The soil skeleton was represented by a critical state bounding surface plasticity model and a (*u*-P) formulation was used to analyze the pore pressure and the displacements. The results exposed that the thickness and the pile length have a small influence on the pile displacements. Contrarily, the natural frequency of the earthquake greatly influences the performance of the system. Considering a 3D soil-pile-structure system, Wang et al. [17] studied the seismic pile moments induced by the inertial and kinematic interaction effects. The soil constitutive model proposed by Wang et al. [18] was utilized. They found that the kinematic interaction dominates the pile moment when the pile head is constrained by the pile cap. When there is no pile cap, the inertial effects dominate the pile moment.

Reliable numerical predictions of seismic response of soil-pile-structure system have to analyze the complete system in a single step accounting for inertial and kinematic interaction. Moreover, dealing with liquefiable soils, fully-coupled formulations are necessary to represent the soil behavior. A number of nonlinear elastoplastic soil constitutive models have been developed in the last years for saturated sand under seismic loading [18–24]. Using the Finn model [21], some authors have investigated the response of soil-piles-structure system dealing with liquefiable soils. For instance, through 2D analyses, Haldar and Babu [25] investigated the failure mechanism in piles and soil-pile interaction. The results showed that the failure pile mode depends greatly on the depth of the liquefiable soil layer, the pile diameter and earthquake predominant frequency. Ren et al. [26] evaluated a 3D numerical model with a group of nine piles supporting a 12-storey concrete frame structure with finite difference analyses. Pore pressure and soil-pile interaction were compared with shaking table test showing a good agreement. Choudhury et al. [27] evaluated the dynamic behavior of a single pile embedded in a homogenous and liquefied soil. The analysis showed that the maximum bending moment occurs at the interface of the liquefiable layer and non-liquefiable layer. López Jiménez et al. [28] explored the seismic response using three dimensional models of a 3-storey reinforced building supported by piles and rigid inclusions. Different soil profiles and frequency excitation were considered. They concluded that the thickness of liquefiable soil, the frequency of earthquake and pile boundary conditions have a great influence on the type of failure in the pile (buckling or bending). In this work, the influence of the sand density was not considered, whereas this parameter is important [2,5,16,25,29].

Despite the capacity of the Finn model to reproduce the main mechanism of liquefaction with a simple formulation, it does not consider the soil density variation during seismic loading. The SANISAND model proposed by Dafalias and Manzari [22] is a comprehensive constitutive model that has the ability to consider this density evolution. It also allows the consideration of the progressive decay in soil stiffness with increasing pore pressure, accumulation of deformation, stress dilatancy and hysteretic loops [29]. It can be used to model the behavior of drained or undrained saturated sand under monotonic and cyclic loading. This model has been utilized by some authors in their investigations [5,29–33]; however, with piles foundation, it has only been used by, [32,34,35]. All of them considered a numerical model with a single pile.

It can be noted that the number of studies considering three-dimensional models of structures supported by pile foundations in liquefiable soils are reduced. A few works consider a complex constitutive model to represent the liquefiable soil. For these reasons, the aim of this study is the analysis of fully coupled three-dimensional soil-pile-structure and soil-inclusion-platform-structure systems (Fig. 1) under seismic loading using the SANISAND model to represent the behavior of liquefiable sand layer. The SANISAND constitutive model is implemented and added as a dynamic linked library (DLL) in the finite difference software Flac 3D [36]. Three different relative density (Dr) values of sand were considered. The behavior of the other soil layers is modeled using the linear elastic perfectly plastic constitutive model with a Mohr-Coulomb failure criterion. A 3-storey reinforced concrete building is modeled over the soil. Two pile lengths are considered. Two benchmark earthquakes are used to study the influence of the frequency excitations in the systems. For each case, the results compare the building response (spectrum response, shear forces, rocking of foundations), the soil response (strains and pore pressures) and rigid element response (bending moments, normal forces and displacements). A calculation with the Finn model [21] is also developed for some cases to compare the excess pore pressure ratio curves. The results show that the frequency of excitation, the relative density of the sand layer and the pile length impacts the soil and structure responses for both systems.

2. Constitutive model for the sand behavior

SANISAND represents a family of Simple ANIsotropic SAND constitutive models developed originally by Manzari and Dafalias [37]. The model is based on a bounding surface plasticity and the critical-state soil mechanics concepts. Later extensions of the model were carried out by Dafalias and Manzari [22], Dafalias et al. [38], Taiebat and Dafalias [39] and Li and Dafalias [40]. The version of Dafalias and Manzari [22] is considered in this study for its simplicity because of the few necessary input parameters. One of the distinctions of this model is that one set of material parameters can be applied to different stresses and densities. The model is suitable to simulate monotonic and cyclic loadings.

The stresses are considered as effective stresses. Both stresses and strains are considered positive in tension and pressure is assumed positive in compression. The mean pressure p is defined by $p = -p_{kk}/3$, the deviatoric stress component is $s_{ij} = \sigma_{ij} + p\delta_{ij}$ where δ_{ij} is the

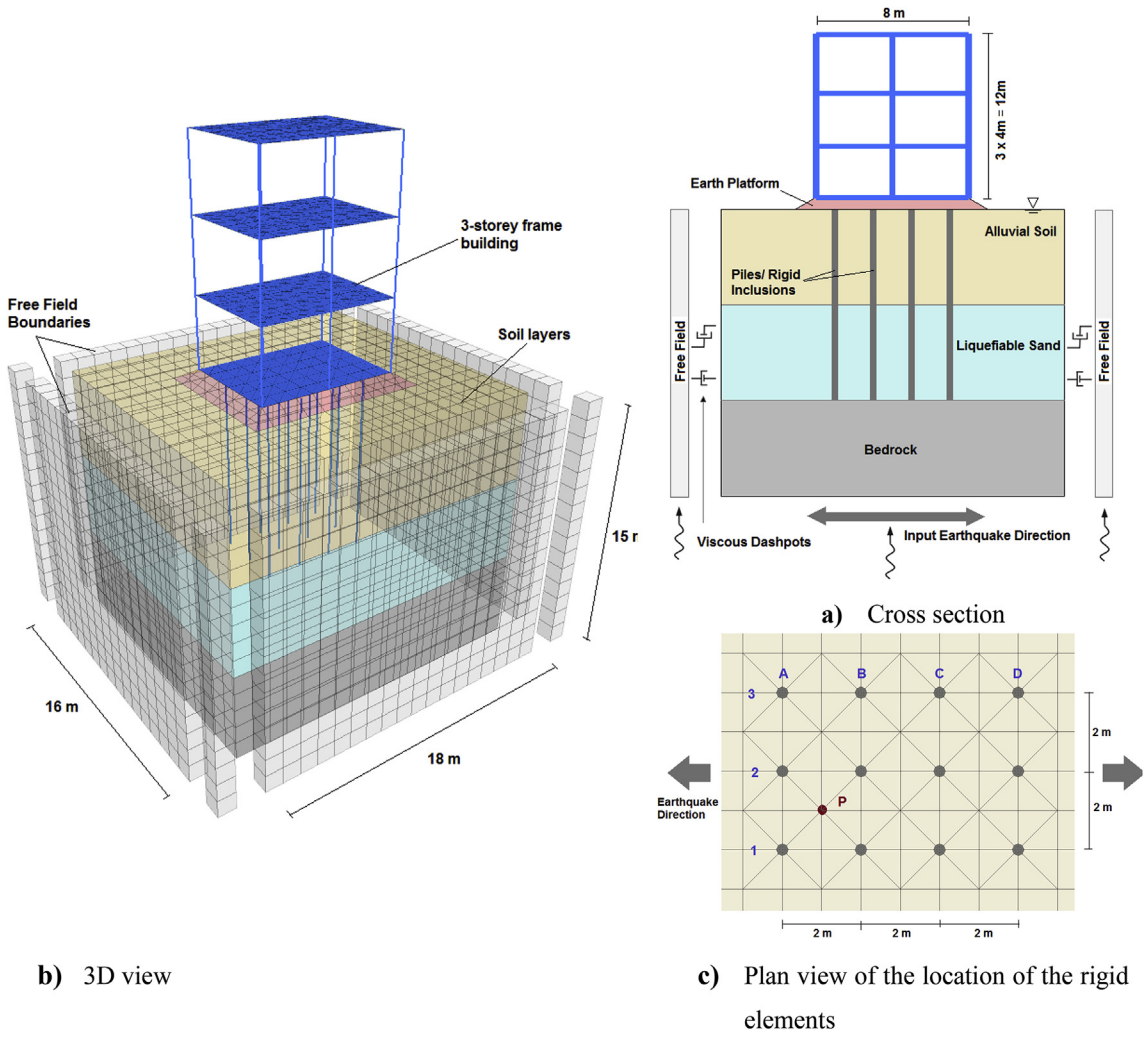

Fig. 2. Geometry of the numerical model.

Kronecker delta function. The equivalent scalar-valued deviatoric stress q is given by $q^2 = (3/2)s_{ij}s_{ij}$. The superscripts e and p denote the elastic and plastic part.

The SANISAND model utilizes a hypoelastic formulation in which the incremental stress and strain tensors are linearly related through variable material moduli that are functions of the current state of stress or strain (Eq. (1)).

$$\dot{\varepsilon}_{ij}^{e} = \frac{\dot{s}_{ij}}{2G}\ \dot{\varepsilon}_{v}^{e} = -\frac{\dot{p}}{K} \tag{1}$$

where ε_{ij}^{e} is the elastic deviatoric strain and ε_{v}^{e} is the elastic volumetric strain defined by $\varepsilon_{ij} = \varepsilon_{ij} - (\varepsilon_{v}/3)\delta_{ij}$ and $\varepsilon_{v} = \varepsilon_{kk}$. The hypoelastic shear and bulk moduli (G and K) are given by Eq. (2), using a dimensionless constant (G_0), the Poisson's ratio (ν), the void ratio (e) and the atmospheric pressure utilized for normalization (ρ_{at}).

$$G = G_0 p_{at} \frac{(2.97 - e)^2}{1 + e} \left(\frac{p}{p_{at}}\right)^{1/2} K = \frac{2(1+\nu)}{3(1-2\nu)} G \tag{2}$$

The location of the critical state line that defines the critical void ratio e_c is given by the Eq. (3) [41].

$$e_c = e_{c0} - \lambda_c \left(\frac{\rho_c}{\rho_{at}}\right)^{\xi} \tag{3}$$

where e_{c0} is the void ratio at $\rho_c = 0$, λ_c and ξ are dimensionless material constants. The distance between the current and the critical void ratio is given by the state parameter $\psi = e - e_c$ [42].

The yield surface is defined by Eq. (4), representing a cone in a multiaxial space. The parameter m controls the size of the yield surface cone, with a small value to develop plastic strain immediately after the application of shearing.

$$f = [(s_{ij} - p\alpha_{ij})(s_{ij} - p\alpha_{ij})]^{1/2} - \sqrt{2/3}\, mp = 0 \tag{4}$$

where α_{ij} is the deviatoric back-stress ratio that characterize the yield surface axis [22,37].

Three concentric and homologous surfaces (dilatancy, bounding and critical surfaces) are considered for the model in the π-plane. The evolution of the dilatant surface is defined by Eq. (5) and the evolution of the bounding surface by Eq. (6). Both are expressed in terms of the state parameter ψ.

$$M^d = Mexp(n^d\psi) \tag{5}$$

$$M^b = Mexp(-n^b\psi) \tag{6}$$

where n^d and n^b are positive material constant and M is the ultimate critical state stress ratio. The dilatancy surface defined by the slope of M^d, allows the model to reproduce contractive volumetric soil response if $s_{ij}/p < M^d$ and dilative volumetric soil response if $s_{ij}/p > M^d$. The bounding surface given by the slope of M^b, permits the model reproduce softening if $s_{ij}/p > M^b$. The lines representing M^d and M^b converge and collapse with the critical surface line M as the sample reaches the critical state and ψ is close to 0.

The Sanisand constitutive model employs a non-associative flow rule to obtain realistic evaluations of plastic strain increments using Eqs. (7) and (8)

$$\dot{\varepsilon}_{ij}^{p} = \mathrm{L}R_{ij} = \mathrm{L}[Bn_{ij} + Cn_{ik}n_{kj} + (D - C)\delta_{ij}/3] \tag{7}$$

$$\dot{\varepsilon}_{v}^{p} = \mathrm{L}D \tag{8}$$

where L is the loading index, $< - >$ the MacCauley brackets (L= L if $L > 0$ and L= 0 if $L \leq 0$). The scalar D associated with the dilatancy is given in Eq. (9) and the values of B and C to take into account the effect of Lode angle on the direction of deviatoric plastic strain rate are given in Eqs. (10) and (11).

$$D = A_d(\alpha_\delta^d - \alpha_{ij}n_{ij}) \tag{9}$$

where A_d is a function of the fabric dilatancy and n_{ij} is the normalized tensor.

$$B = 1 + \frac{3}{2}\frac{1-c}{c}g(\theta, c)\cos 3\theta \tag{10}$$

$$C = 3 + \sqrt{\frac{3}{2}}\frac{1-c}{c}g(\theta, c) \tag{11}$$

where c is the material constant denoting the ration of the triaxial extensive strength to compressive strength with θ the Lode angle.

3. Numerical modeling

3.1. Soil mesh

In this study, the soil volume dimensions considered are 18 × 16 × 15 m. The analyses are carried out considering a soil profile that is composed of 3 layers of 5 m each, where the layer in between corresponds to the liquefiable sand and the other layers are not liquefiable layers (Fig. 2). The upper layer corresponds to an alluvial soil and the lower layer corresponds to the bedrock [30]. The water table is located at the surface ground level. The properties of the different layers are shown in Table 1. The behavior of the non-liquefiable soils is represented by the elastic perfectly plastic model with a Mohr-Coulomb failure criterion and the one of the liquefiable soil with the SANISAND constitutive model [22]. This model has shown the ability to reproduce a series of monotonic and cyclic tests on Nevada sand [33,43]. The material parameters required by the model are displayed in Table 2 [29,32], divided into six categories based in their functions. Relative density (Dr) of 40%, 55% and 80% are considered as input parameters of the Sanisand constitutive model (liquefiable sand).

Fig. 2a shows the mesh discretization of the system. The soil mesh is constituted by 8300 hexahedral zones [44]. In this case, the maximum size of the mesh elements is equal to 1 m. This size allows an accurate representation of the wave transmission through the model, the highest frequency that can be modeled is 6 Hz [45]. Artificial boundary conditions are used in the soil mesh sides to represent in a correct way the semi-infinite nature of the soil deposits [46]. During dynamic calculations, free-field boundaries are applied on the sides of the soils mesh. Using this process, there is no distortion in the plane waves propagating upward the boundaries [47]. This secondary grid is coupled to the main grid by viscous dashpots (Fig. 2a). Rigid condition is applied to the mesh base in order to apply the earthquake input motion.

Table 1
Soil material properties [25,30].

Soil Layer	Alluvial	Liquefiable Sand	Bedrock
Density, ρ_{sat} (kg/m^3)	2020	1962	2373
Poisson's ratio, ν	0.26	0.45	0.31
Shear modulus, G (kPa)	1.99×10^5	2.7×10^4	1.15×10^6
Cohesion, c (kPa)	0	0	0
Friction angle, ϕ (°)	35°	33°	40°

For the rigid inclusions systems, there is a 0.60 m thick earth platform between the soil and the structure. The material properties of the mattress are shown in Table 3. The linear elastic perfectly plastic constitutive model with a Mohr-Coulomb failure criterion is utilized to represent the behavior of the earth platform.

The liquefiable layer (SANISAND model) is considered using a low Rayleigh damping of 0.5% to reduce the high frequency noises [30,31]. However, for the elements where the linear elastic perfectly plastic constitutive model with a Mohr-Coulomb failure criterion is implemented, an additional damping is introduced in the elastic part of the response where there is no energy loss in the soil during the dynamic analysis. A Rayleigh damping with a ratio of 5% for a central frequency equal to 2.75 Hz is used. This frequency corresponds to the first soil deposit mode [48,49].

The use of the SANISAND constitutive model is compared in some calculations with the simpler Finn constitutive model [50]. This model, implemented in FLAC for simulating liquefaction, is based on the linear elastic perfectly plastic (with a shear failure criteria of Mohr Coulomb type) constitutive model. Pore pressure generation is modeled by computing volumetric strains induced by the cyclic shear strains using a formulation given by Byrne [21]. The details of the formulation are not displayed here. The material properties for the Nevada sand to use the Finn constitutive model are displayed in Table 4.

3.2. Vertical reinforced elements

A group of 12 piles or rigid inclusions elements embedded in the soil are considered in the analyses. The distribution of the rigid elements is shown in Fig. 2c. Each concrete element has a 0.30 m diameter. The properties of the reinforced elements are displayed in Table 5. The coverage ratio, which is the proportion of the total area covered by piles, is equal to 1.7% [51–54]. Two reinforced element lengths (10 m or 14 m) are considered. The behavior of the piles or inclusions is considered as linear elastic in all calculations.

In this study, the reinforced elements are modelled with beam structural finite elements perfectly bonded with the soil [19,30,35,55]. Any mesh refinement around the pile was considered accepting some loose of accurate distribution of stresses and displacements. This additional refinement does not significantly affect the results and increases a lot the computation time. Although this technique allows obtaining the pile efforts directly from the analysis, it does not consider the physical cross section of the pile. According to Kitiyodom et al. [56] and Wotherspoon [57], this technique results in greater displacements and bending moments along the pile than with the method where the reinforced element is considered as solid elements. With the purpose of comparing how the physical cross section influences the generation of pore pressure in the analyzed systems, some calculation were developed with a hybrid technique. In this method, the pile is represented by solid elements and a beam element is introduced at the piles center axis [58,59]. To avoid a modification of the pile response with the beam element introduction, the flexural rigidity of the beam element (EI) is reduced [58]. The consideration of the solid elements to model the pile or rigid inclusion elements implies a reduction of the time step, leading to a computation time increase.

3.3. Superstructure

A 3-storey reinforced concrete building is placed over the considered soil profile (Fig. 2). The structure is composed of two bays of 4 m and one span of 6 m. The storey height is equal to 4 m (Fig. 2a). The sections of the structural element are shown in Table 6. The columns and slabs are considered made of reinforced concrete with the same material properties as for the vertical reinforcement elements (Table 5). The behavior of the structural elements is considered as linear elastic.

The columns and floor slabs are modelled by a collection of beam

Table 2
Material parameters used in SANISAND constitutive model for Nevada Sand [29,32].

Parameter function	Elasticity		Critical state					Dilatancy		Kinematic	Hardening		Fabric dilatancy	
Index	G_0	ν	M	c	λ_c	e_0	ξ	A_0	n^d	n^b	h_0	c_h	Z_{max}	c_z
Value	150	0.05	1.14	0.78	0.027	0.83	0.45	0.81	1.05	2.56	9.7	1.02	5.0	800

Table 3
Material properties considered for the earth platform.

Properties	Young modulus (MPa)	Shear Modulus (MPa)	Volumic Weight (kg/m^3)	Damping Ratio	Cohesion (kPa)	Friction angle (°)	Wave velocity (m/s)
Platform	50	19	2000	0.05	50	25	160

Table 4
Nevada Sand properties [25].

Properties	Unit	Dr = 40%	Properties	Unit	Dr = 40%
Poisson's ratio, ν	–	0.45	p_0	kPa	100
Shear modulus, G	kPa	2.7×10^4	K_0	–	0.5
Bulk modulus, K	kPa	2.16×10^5	$(N_1)_{60}$	–	7.2
Permeability, k	m/s	6.6×10^{-5}	Mean effective vertical stress, σ'_{vo}	kPa	167
Porosity	–	0.424	Bulk modulus of water, k_w	kPa	2.51×10^6
Friction angle, ϕ	°	33°	Soil density (ρ_{sat})	kg/m^3	1962

and shell structural elements respectively. The first ones are straight segments of uniform bisymmetrical cross-sectional properties lying between two nodal points (six degrees of freedom per node) and the second ones are three noded (15 degrees of freedom) flat finite elements which resist to bending and membrane loading. The foundation slab is represented by liner elements. These elements have the same properties as shell elements and additionally consider the interface behavior with the soil through linear springs with finite tensile strength in the normal direction and a spring-slider in the tangent plane to the liner surface. The installation of the superstructure is considered in a single phase after the model equilibrium. Rayleigh damping with a factor of 5% and model coefficients α= 0.6583 and β= 0.0037 calculated based on the first and second mode frequencies of the superstructure are used to simulate the structural damping. The fundamental period of the structure in fixed condition is equal to 0.493 s.

4. Input motions

The Loma Prieta 1989 and Northridge 1994 earthquake motions are imposed to the numerical model. The characteristics of the earthquakes are shown in Table 7. Although the duration of the earthquakes records are long, only 4 s (between 2 and 6 s for the Loma Prieta earthquake and between 7 and 11 s for the Northridge earthquake) of each earthquake record are applied in the horizontal direction to all nodes in the bottom part of the model. They both were scaled to the same peak acceleration value (0.75 g) with the idea of obtaining a rapid liquefaction. The signals were treated with baseline correction and a low-pass filtering (10 Hz). Fig. 3 shows the only 4 s acceleration time-histories applied.

5. Numerical cases

Table 8 displays the soil-pile-structure and soil-inclusion-platform-structure cases analyzed in this paper. The cases are represented schematically in Figs. 4 and 5. The name of each case has two terms, the first term (RI or P) refers to Rigid Inclusion or Pile case, the second one indicates the rigid element length (10 m or 14 m). The term w/S refers to cases without structure. For instance, the case RI-10 m corresponds to the rigid inclusions system of 10 m pile length. For comparison, a case with the Finn constitutive model for the liquefiable sand layer was also analyzed. This case will be identified with an additional term (F) in its name. As mentioned before, the modeling of reinforced elements was developed with the only beam structural element technique for all cases. Additionally, some cases were analyzed with the hybrid technique (*). The time calculation for the first one is around 23 h and for the systems that consider hybrid modelling was around 180 h for each case. For reference in this text, all the calculations were developed using a computer with a core i7 3.6 GHz 64-bit processor and 8 Gigabytes of RAM.

Table 6
Sections considered in the building.

Section	Notation	Length (m)	Width (m)	Thickness/height (m)
Floor slab	h_{fs}	8	6	0.25
Foundation slab	h_s	8	6	0.25
Columns	a_c	0.4	0.4	4

6. Procedure of analysis

The analyzed systems are developed using Flac 3D, which uses an explicit time-integration scheme, a fully coupled solid-fluid interaction and is able to solve dynamic problems. A former mechanical equilibrium state is obtained with the groundwater level present at the soil surface. Then, the vertical reinforcements are installed. The last static calculation step considers the activation of the earth platform and of the surface structure. In all these preliminary steps, all material groups were considered with the linear elastic perfectly plastic constitutive model with Mohr-Coulomb shear failure criterion and no fluid flow is considered to obtain a faster solution.

After that, a flow calculation is carried out to determine the steady flow condition. Then the SANISAND model was assigned to the potentially liquefiable sand layer and a final mechanical calculation is done subsequently. The fluid flow is prevented since the consolidation process is not the main concern.

The dynamic analysis is then performed as a coupled simulation (fluid and mechanical interaction). At this stage, a value of 2 GPa for

Table 5
Rigid element properties.

Properties	Diameter (m)	Cross-sectional area (m^2)	Moment of inertia (m^4)	Young's modulus (GPa)	Shear Modulus (GPa)	Volumic Weight (kg/m^3)	Damping Ratio
Rigid elements	0.30	0.0706	0.000398	30	12.5	2500	0.05

Table 7
Earthquakes base motions considered.

Earthquake	Date	Duration (s)	Peak ground acceleration PGA (m/s^2)	Magnitude (Mw)	Predominant Frequency (Hz)
Loma Prieta, USA	1989/10/17	40	4.69	7.1	1.35
Northridge, USA	1994/01/17	30	8.65	6.7	4

the water bulk modulus was used. The permeability coefficients considered are respectively 6.6×10^{-5}, 6.05×10^{-5} and 3.7×10^{-5} m/s for Dr = 40%, 55% and 80%. The formulation of the coupled analysis is done within the framework of the quasi-static Biot theory (single-phase Darcy flow in a porous medium). For the dynamic calculations, the lateral boundaries are changed to free field boundaries and the corresponding horizontal wave using acceleration is applied at the base of the models.

7. Results

The results of the calculations are presented in this section. Concerning the building, the spectrum response, the shear forces and the rocking of foundation are presented. For the soil response, pore pressures and strains are displayed at different depths. Finally the response of the rigid vertical elements is given in terms of bending moments, normal forces and displacements. The values presented in this section correspond to the maximum values in the calculation. However, concerning the piles result, the maximum values of the envelope of the elements located in axe 1 (Fig. 2c) are considered. The higher efforts are located in this axis.

7.1. Structure response

7.1.1. Response spectrum

A seismic soil-structure interaction analysis evaluates the overall response of the superstructure, the foundation and the soil underlying and surrounding the foundation, for a specific ground motion. In order to verifier the influence of the soil-structure interaction on the soil movements, the response spectrum of the ground motions recorded at the base of the structure (ground surface) for all cases are presented in Fig. 6. The Fast Fourier Transform is used to calculate the acceleration response spectrum. These spectrums denote the peak acceleration of a single-degree of freedom system with 5% of damping for a specified earthquake ground motion. Considering the knowledge of structural dynamics, the response spectrums are usually used for the design of structures and calculate the shear forces in building codes in terms of the natural frequency of the system. It can be noted from Fig. 6 that for all the analyzed cases, the spectra are reduced because the surface acceleration records are lowered compared to the input record applied at the bottom of the model. This decrement is due to the fact that the liquefied layer attenuates the energy as the motion propagates to the surface and inhibits liquefaction in the shallower soil [10,29,60–62]. However, the response spectrum increases when the relative density of the sand layer is augmented and the attenuation given by the liquefaction triggering is reduced (Fig. 6b). However, there is still some attenuation caused by the soil resistance degradation due to the induced shear strains [63].

The length of the rigid vertical elements influences the seismic motions characteristics at the base of the structure by altering the kinematic and inertial interactions. The spectrum responses are increased in the systems with 14 m pile length compared to the ones with 10 m pile length, mainly for short periods (Fig. 6a). At the same periods, the consideration of the superstructure significantly increases the spectrum response. Similar results were reported by Maheshwari and Sarkar [15]. It is also noticeable in Fig. 6a that the responses of the RI-10-F and P-10-F systems are greatly decreased in lower and large periods compared to the systems with SANISAND model. It can be observed that the responses of the pile systems are greater than the rigid inclusion ones.

The response spectrum of the RI-10 m and P-10 m systems excited by the Loma Prieta earthquake are greater compared to the responses obtained with the Northridge earthquake (Fig. 6c). This implies that the response increases when the frequency of the excitation decreases.

7.2. Shear forces in the superstructure

The pile or rigid inclusion foundations influence the amount of energy absorbed by the structure during earthquakes. Fig. 7 shows the comparison of the shear forces developed in the building. The shear forces in every column were summed up in every time increment of the time history analysis to obtain the maximum shear force at each level. Then the absolute maximum value of the shear forces in each level is recorded. The response of the fixed-base case (F–B) is also shown. In the F–B case, the superstructure is analyzed with fixed support conditions and without soil. It is visible from Fig. 7 that the consideration of the SSI reduces the shear forces in the superstructure compared to the fixed-

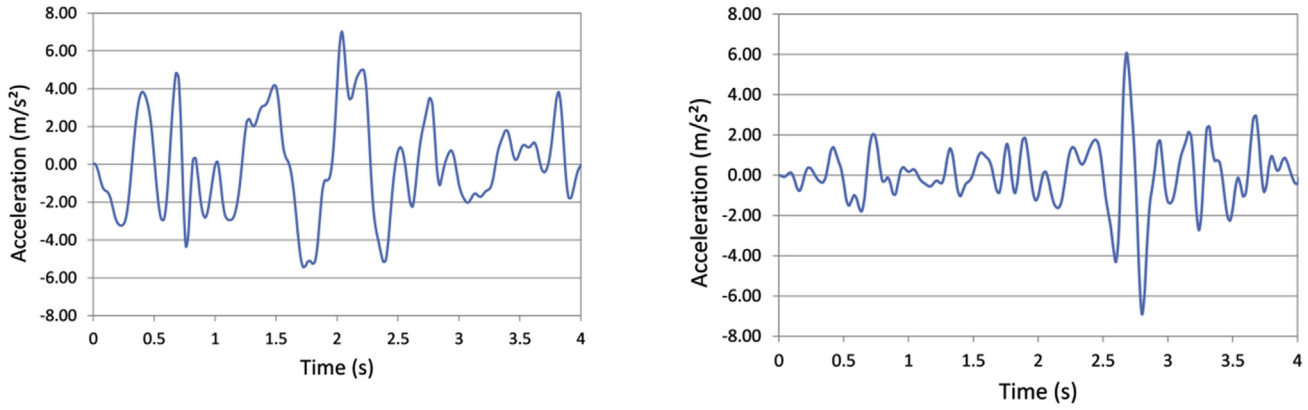

Fig. 3. Original earthquake records.

Table 8
Characteristics of the analyzed cases.

Rigid elements	Name of Case	Pile Length (m)	Structure	Liquefiable soil		Earthquake
				Constitutive model	Dr	
Rigid inclusions systems	RI-10 m[a]	10	Yes	SANISAND	40, 55, 80%	Loma Prieta/Northridge
	RI-10 m w/S	10	No		40%	Loma Prieta
	RI-14 m[a]	14	Yes		40%	Loma Prieta/Northridge
	RI-10m-F	10	Yes	Finn	40%	Loma Prieta
Pile systems	P-10 m[a]	10	Yes	SANISAND	40, 55, 80%	Loma Prieta/Northridge
	P-10 m w/S	10	No		40%	Loma Prieta
	P-14 m[a]	14	Yes		40%	Loma Prieta/Northridge
	P-10m-F	10	Yes	Finn	40%	Loma Prieta

[a] Cases analyzed additionally with the hybrid technique to model the pile or inclusion.

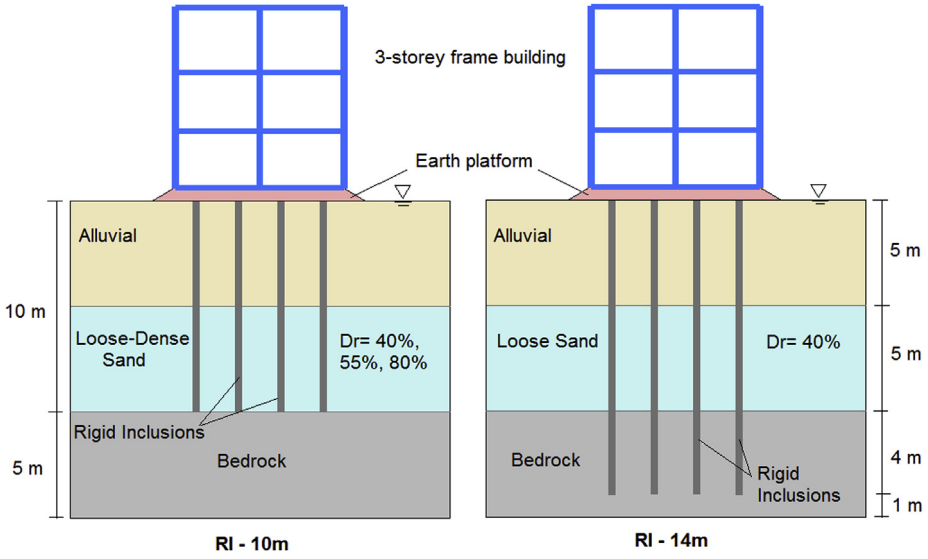

Fig. 4. Soil - rigid inclusions - earth platform - structure analyzed systems.

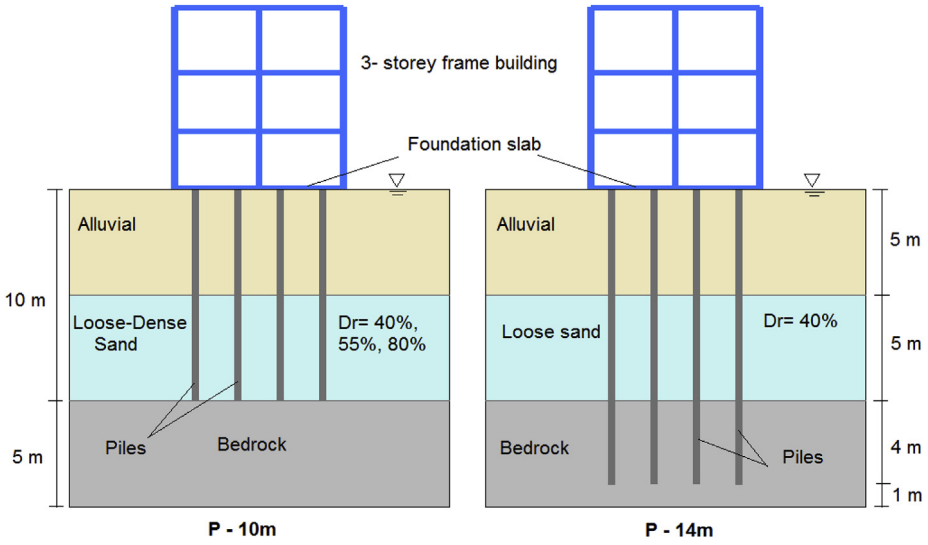

Fig. 5. Soil - piles - structure analyzed systems.

base case. In general, the storey shear forces in the building with pile systems are greater than in the rigid inclusion systems considering the same pile length. This occurs due to the fact that the inertial forces are increased due the pile head rigid connection with the foundation slab.

In the analyzed systems, the shear forces in the P-14 m case are greater than in the cases with the 10 m pile length (Fig. 7a). This happens because the longer piles are subjected to inertial forces from the embedded part in the bedrock. However, considering the rigid inclusion cases, the RI-10 m system shows larger shear forces compared to the RI-14 m one. There is no connection of the rigid elements with the slab foundation and also the ground accelerations are larger for the RI-10 m case.

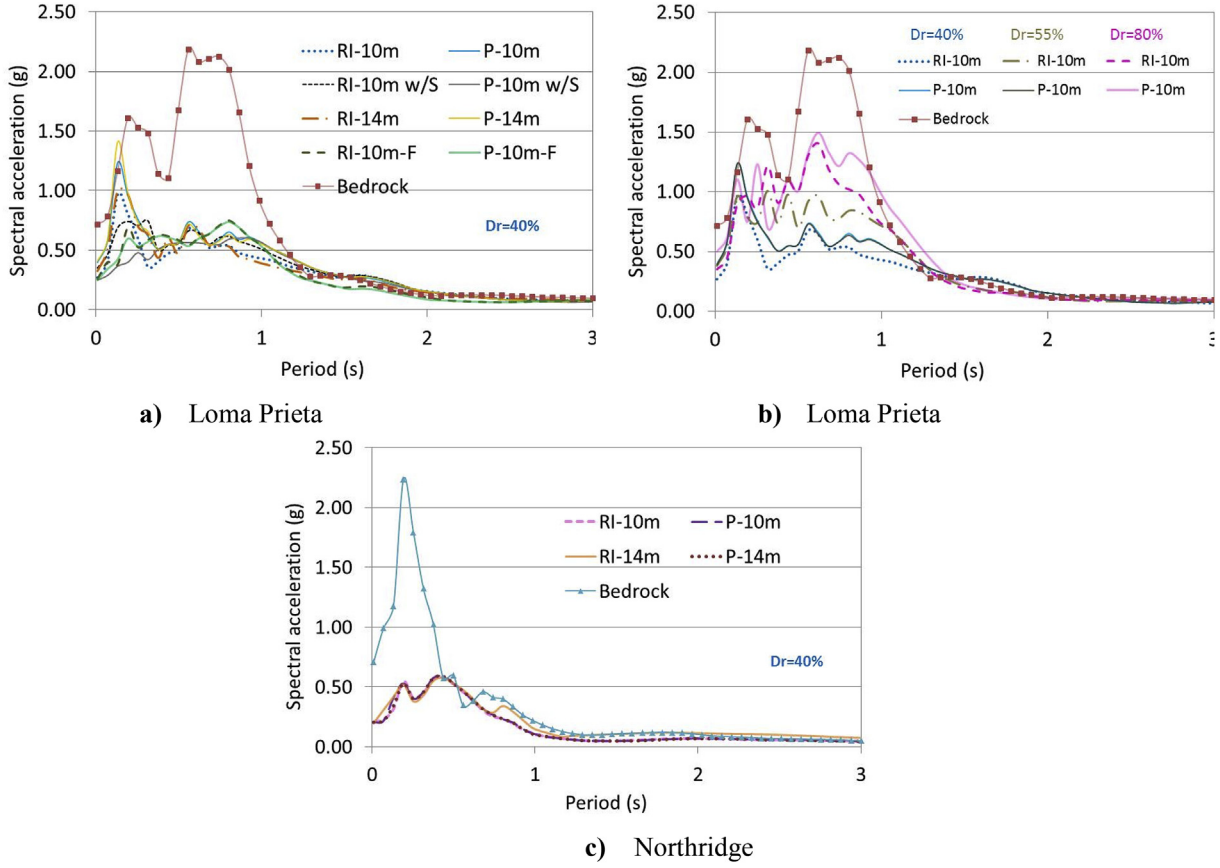

Fig. 6. Acceleration response spectrum of the analyzed systems for different conditions and earthquakes.

The shear forces in the building of the systems analyzed with the Loma Prieta earthquake are larger than the ones with the Northridge earthquake using the same characteristics (Fig. 7a and b). This is explained by the fact that the fundamental period of the system lies in a response spectrum region where the spectral acceleration is larger than with the Northridge earthquake.

As expected and in accordance with the spectrum responses, the shear forces are increased as the relative density increases in the pile cases (Fig. 7c). However, for the rigid inclusion cases, the shear forces are less influenced by the relative density. The RI-10 m case with Dr = 40% shows the greater values.

7.3. Rocking of foundations

Rocking occurs when the inertial forces generated in the superstructure cause compressions in one side (settlements) and tensions

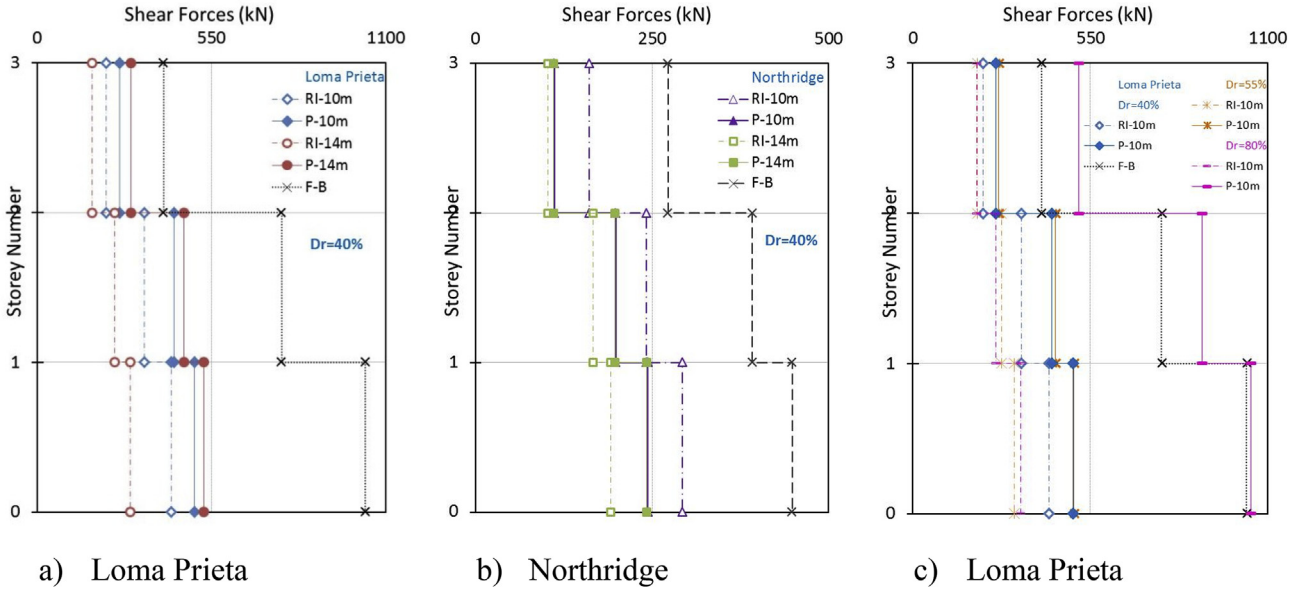

Fig. 7. Maximum shear force distribution on the analyzed systems for different conditions and earthquakes.

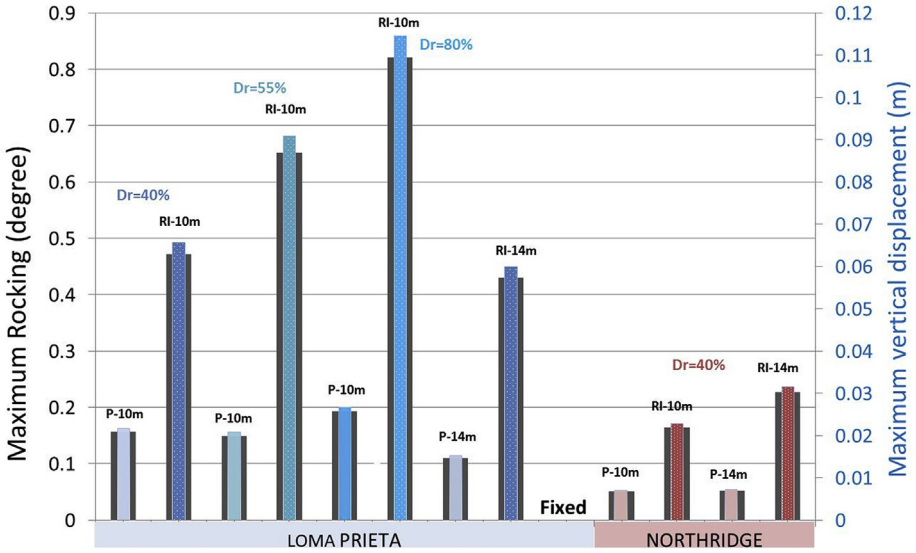

Fig. 8. Maximum rocking and vertical displacements for different conditions.

(uplifts) in the other side of the foundation during strong seismic excitations. The rocking can affect the stability of the building due to the lateral displacement increase. On the other hand, some of the seismic energy can be dissipated due to the rocking-dissipation which reduces the shear forces in the structure. The amount of rocking depends on the foundation type supporting the superstructure. In this study because in the analyzed cases, the rigid elements are placed or anchored on the bedrock, the axial deformation of the elements and the deformation of the surrounding soil are the main factors which can cause rocking.

Fig. 8 displays the maximum rocking in the systems. There is no rocking in the fixed-base structure (F–B). In general, the rocking values in the rigid inclusion cases are greater than in the pile systems with the same pile length and relative density. For instance, the maximum rocking values in the P-10 m are respectively equal to 0.15° and 0.47° for the RI-10 m with a 40% relative density. For Dr = 80%, the same values are obtained, respectively 0.19° and 0.82°. This is because in the pile systems, the building are directly connected to the slab foundation and in the rigid inclusion systems, there is the presence of the earth platform. The rocking in the P-10 m system (0.15°) is greater than in the P-14 m case (0.11°) with a 40% relative density and the Loma Prieta earthquake. The anchorage on bedrock of the P-14 m case reduces the foundation uplift and the settlement values when the compression forces act on the other side of the foundation. A similar behavior is obtained for the systems with the Northridge earthquake. However, the rocking of the P-10 m and P-14 m cases analyzed with the Loma Prieta earthquake are 67% and 54% greater than with the Northridge earthquake one.

The rocking values are decreased in the systems as the values of relative density are reduced. For instance, the rocking values for the RI-10 m case with 80%, 55% and 40% of relative density are respectively equal to 0.82°, 0.65° and 0.47°.

7.4. Soil response

7.4.1. Pore pressure

To study the soil response, the pore pressure time histories computed between the rigid vertical elements at point P (Fig. 2c) at two depths (7 m and 9 m) are displayed in Fig. 10. Except for the Fig. 9e, all the plots shown in this section consider 40% of relative density for the sand layer (at 5–10 m depth). The presence of the loose layer causes a stronger contractive response during the dynamic loading which in turns produces a faster increase of the excess pore pressure and a decrement of the vertical effective stress and stiffness. In this study, the excess pore water pressure ratio (r_u) is defined as the ratio of the difference of pore pressure in a specified stage (u) and the initial pore pressure (u_0) over the initial effective stress (σ'_0). If $r_u = 0$, the pore pressure is equal to the applied back pressure. However, when $r_u = 1$, true liquefaction takes place if the total stresses are kept constant during the cyclic loading. In a range of excess pore pressure (r_u=0.8–1), there is a development of large strains and the cyclic mobility occurs [60,64]. In this study the triggering liquefaction is assumed when $r_u = 0.8$.

The pile and inclusion cases analyzed with Dr = 40% for the liquefiable soil layer under the Loma Prieta earthquake are shown in Fig. 9a and b. It is clear from these figures that there is a greater increment in excess pore pressure in the P-14 m case compared to the P-10 m one. It is also noticeable that this increment is more pronounced in the rigid inclusion cases than in the pile ones. After the first second of calculation, all the systems experience an important drop of the r_u values even to negative values (R-10 m case in Fig. 9a). These drops in excess pore pressure are due to the excessive dilatation tendency of the SANISAND model [5,29].

The frequency and amplitude of the motion have a great influence in the excess pore pressure ratio time histories [60]. Fig. 9c and d shows the impact of the excitation frequency in the development of liquefaction at different depths. It can be noted that the excess pore pressure ratio values of the pile or inclusion systems with the Northridge earthquake (4 Hz) are smaller than with the Loma Prieta earthquake (1.35 Hz), except for the RI-10 m case at 7 m depth (Fig. 9c)). For all the analyzed cases under the Northridge earthquake, the drops in r_u values are importantly reduced compare to the ones with the Loma Prieta earthquake. It is important to note that in the cases analyzed with the Northridge earthquake, the drops in excess pore pressure were highly decreased.

Fig. 9e presents the excess pore pressure ratio histories for the P-10 m case with different Dr values of the sand layer (at 7 m depth). As expected, the r_u values increase as the relative density value decreases. Only the cases analyzed with Dr = 40% and 55% got true liquefaction. The system analyzed with Dr = 80% shows an important delay in the pore pressure development compared to the cases with lower relative densities. A similar behavior is shown in Fig. 9f for the RI-10 m at 9 m depth. In this case, only the Dr = 40% case implies a true liquefaction. Other comparisons of pile and rigid inclusion systems with the 40% and 80% relative density at 7 m and 9 m depth are respectively displayed in Fig. 9g and h.

The generation of excess pore pressure in the numerical calculations

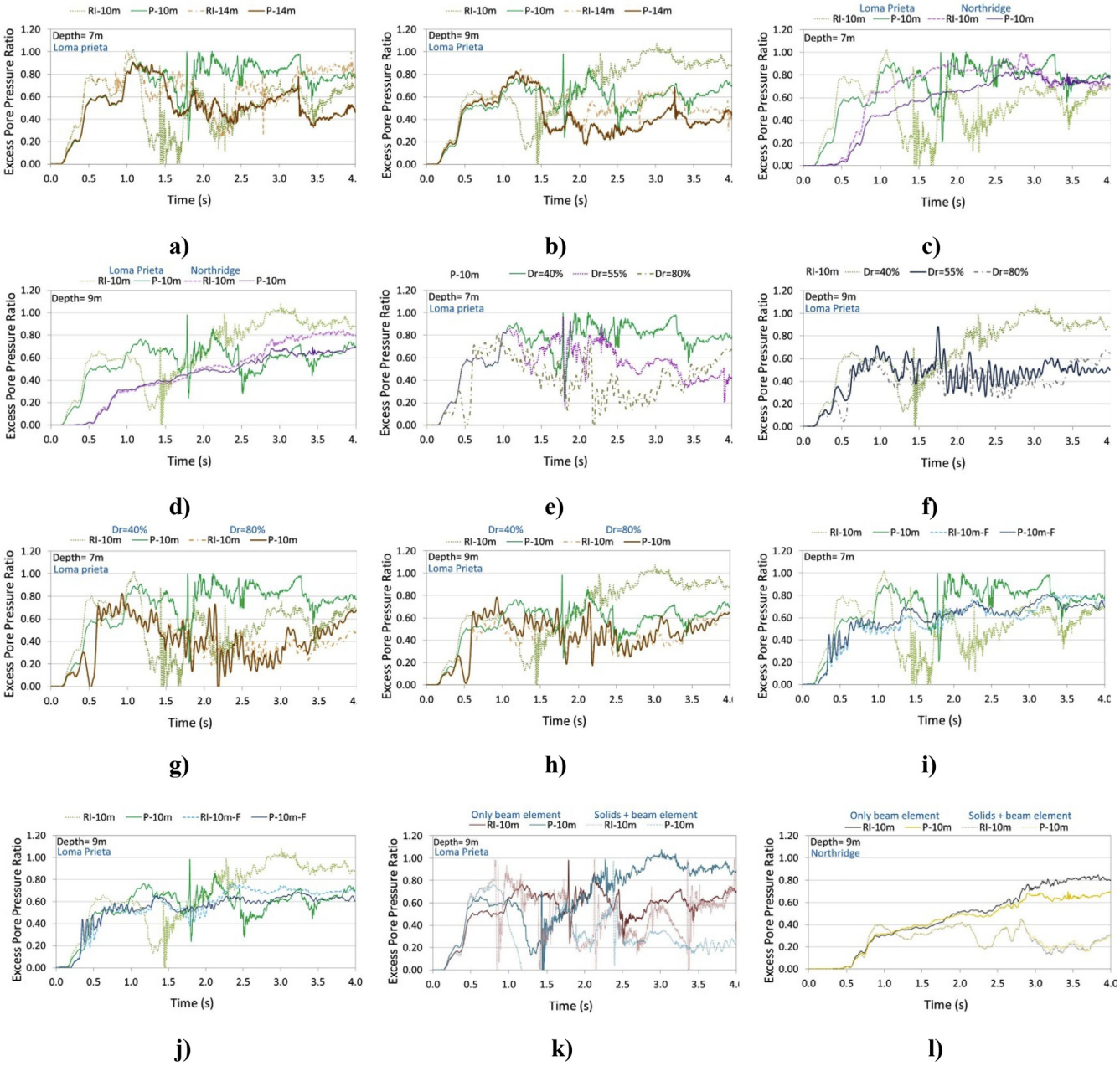

Fig. 9. Excess pore pressure ratio time histories in the analyzed systems at different depths.

developed with the SANISAND model are compared to the ones obtained with Finn model in Fig. 9i and j. The generated results of excess pore pressure in the P-10 m system at 9 m depth with the SANISAND and Finn model are similar, but not for the RI-10 m case (Fig. 9j). Nevertheless, for the analyzed cases at 7 m depth, the systems analyzed with the SANISAND model got true liquefaction while the cases analyzed with the Finn model get a maximum value of r_u equal to 0.8 (Fig. 9i). This could be due to the limitations of the Finn model which cannot correctly reproduce the cyclic mobility response mechanisms and the associated pattern of shear strain accumulation or due to the fact that the rearrangement of particles cannot be considered [18,20,23,65]. It can be noted that at the beginning of the curves in Fig. 9h, j, the generation of excess pore pressure (around 0.2–0.4 s) with the SANISAND model is gradual; whereas with the Finn model the rapid changing in pore pressure results in steeper curves which occurs because the pore pressure in this model are developed due to plastic deformations of soil and it affects the stiffness and strength of the sand [66].

Fig. 9k,l shows how the consideration of the physical cross section of piles affects the development of excess pore pressures. It is noticeable that during the first second of calculation, the systems in which the piles were modeled with the hybrid method got smaller r_u values compare to the same systems where piles were modelled with only beam elements. However, as the analysis continues, the excess pore pressure values of the cases analyzed with the hybrid method are larger. This could be explained by the fact that the physical cross section of the pile increases the confining pressure.

7.5. Shear strains in the ground

Fig. 10 shows the maximum shear strains values recorded at point P (Fig. 2c) at different depths. The maximum values are importantly increased in the two upper layers compare to the values in bedrock. In the upper layer (0–5 m depth), the shear strains increase for the rigid

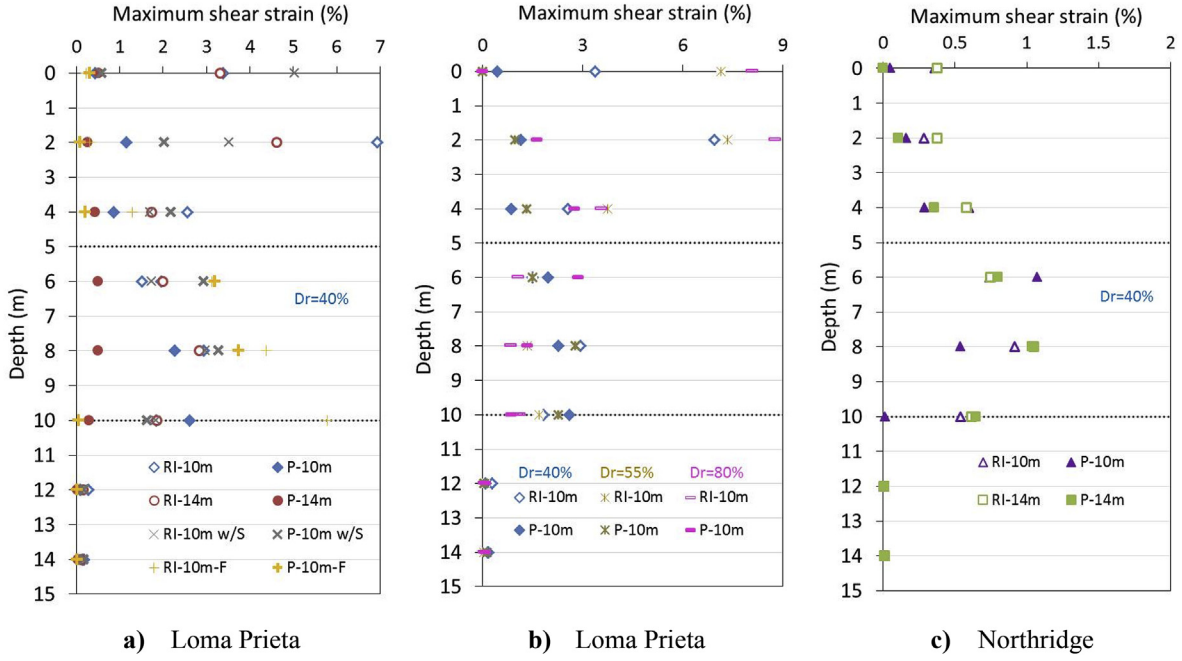

Fig. 10. Maximum shear strain in the analyzed systems for different conditions and earthquakes.

inclusion cases compared to the pile cases under the Loma Prieta earthquake (Fig. 10a and b). The rigid connection of the piles with the slab foundation or the free condition at the inclusion head seems to have an important influence on the development of shear strains in the upper part of the model. The shear strains in the liquefiable soil layer analyzed with a 40% relative density are greater for the rigid inclusion cases than for the pile ones (Fig. 10a).

It is noticeable from Fig. 10 (b) that the increase of soil relative density implies a decrease of the shear strain level. Similar results were obtained by Haldar and Babu [25]. For instance the maximum shear strain reached in the RI-10 m with a Dr = 40% is around 3%, which is reduced of 1.1% for the case with Dr = 80%. For the P-10 m case the values are respectively reduced from 2.3% to 0.85% for Dr = 40% and Dr = 80%.

Comparing the results of Fig. 10a and c, it is evident that the shear strain values decrease when the predominant earthquake frequency is increased (same peak acceleration). This remark is in accordance with Haldar and Babu [25].

7.6. Rigid vertical element response

7.6.1. Bending moments

The maximum bending moment values obtained in the pile and rigid inclusion elements are displayed in Fig. 11. The bending moments in the rigid inclusion heads are null because of the earth platform presence. However, in the pile heads, the moments are important due to the fixed connection with the foundation slab that amplifies the inertial forces. These forces are predominant before liquefaction at this level [67].

In the cases where the superstructure is not considered, the high moments near the pile head are inhibited (Fig. 11a). However, the moments in the bottom remain close to the values with the structure presence which implies that similar kinematic forces are developed in both cases [16].

The pile length has a small influence on the repartition of bending moments along the rigid elements in the upper layer (0–5 m depth). However, it can be noted that the moments from 5 to 10 m depth (except at 6 m depth) are greater for the systems with 14 m rigid elements length (Fig. 11a). For instance at 7 m depth, the moments in the RI-14 m are 59% greater than the RI-10 m ones. In the piles cases, a difference of 37% is obtained. Similar results can be obtained for the systems analyzed with the Northridge earthquake.

In this study, as the thickness of the liquefiable layer is greater than one-third but less than two-thirds of the total thickness of the soil deposit, the maximum moment (in most of the cases) is located at the interface of the liquefiable and non-liquefiable soils (5 m and 10 m) for the fixed-head pile, otherwise the maximum value is located at the pile head [1]. For example, for the case with 14 m rigid element length, the values are respectively equal to 245 kN.m and 276 kN.m for the RI-14 m and P-14 m at 11 m depth (Fig. 11a). These peak values are mainly due to the kinematic forces and are similar in the pile and inclusion cases. Similar behavior is presented for the cases analyzed with the Northridge earthquake (Fig. 11c). This agrees with the results presented by Choudhury et al. [27], Finn and Fujita [68], Janalizadeh and Zahmatkesh [14], Phanikanth et al. [13] and Rahmani and Pak [16].

Fig. 11b compares the systems analyzed with different relative densities under the Loma Prieta earthquake. In the liquefiable soil layer, the bending moments in the rigid inclusion cases decrease as the relative density value increases. For instance, the moment (88 kN.m) in the inclusion case at 8 m depth with Dr = 40% is respectively reduced by 13% and 18% compared to the cases Dr = 55% and 80%. These values are also in accordance with the pore pressure results (Fig. 9), which indicates that the pore pressure decrease (due to dilatation) tends to reduce the pile bending moments [1]. For the pile case, a similar behavior is observed with a difference that the values with Dr = 55% are equal or greater than the values with Dr = 40%. However, this tendency is contrary in the upper layer, where the moments in the pile or inclusion systems are greater with a higher relative density. The great influence of the inertial forces in the superstructure increases the shear forces at the base of the building, when the relative density increases (Fig. 7b).

The influence of the frequency excitation on the response of the rigid elements can be observed by comparing values of Fig. 11a and c. The increase of the frequency implies an average decrement of respectively 69% and 67% in the bending moment values for the RI-14 m and P-14 m cases at different depth. Same differences - respectively of 67% and 65% - for the RI-10 m and P-10 m cases are obtained. Analogous results are obtained by Liyanapathirana and Poulos [1] and

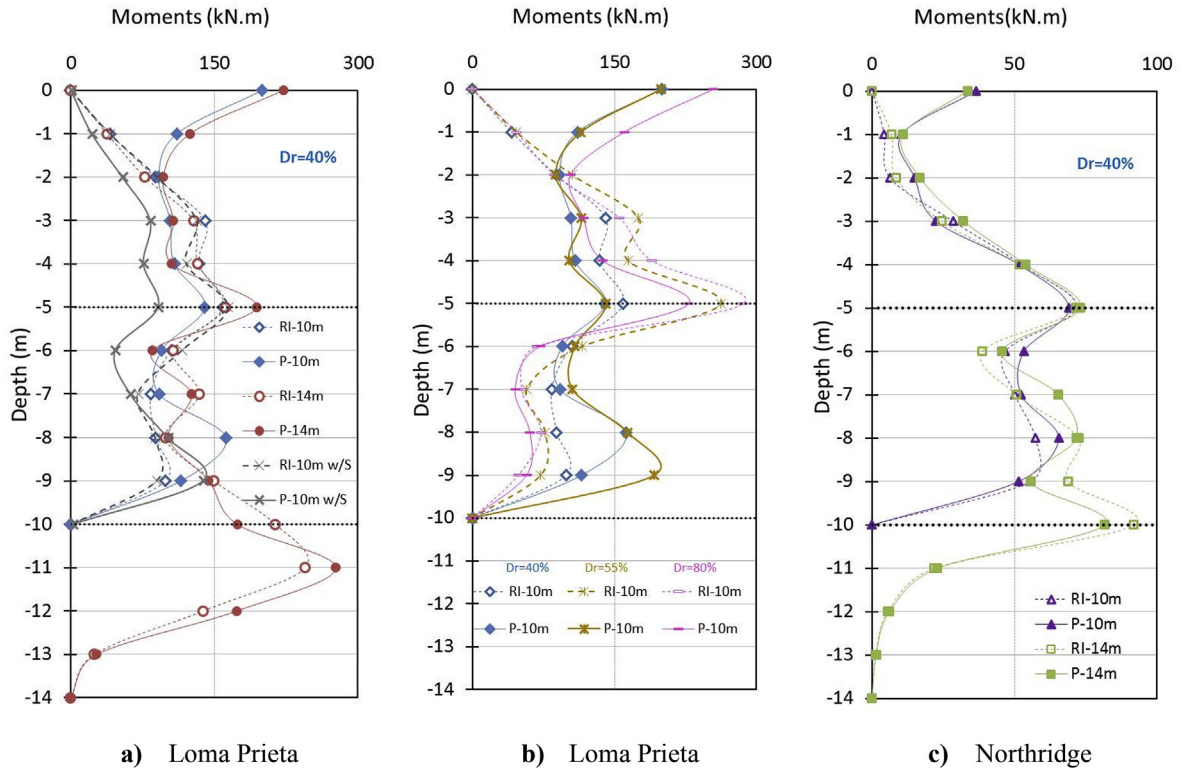

Fig. 11. Normal forces in rigid inclusion and pile systems for different soil profiles and earthquakes.

Rahmani and Pak [16].

7.7. Normal forces

Fig. 12 shows the maximum normal forces in the rigid elements. For all cases, the normal forces in the pile cases are greater than in the rigid inclusion systems. This difference is maximal at the structural element head. The inertial forces are lower in the rigid inclusion systems due to the presence of the earth platform and there is no connection with the foundation slab. For instance, the normal force in the P-10 m case is 84% smaller than in the RI-10 m case (Fig. 12a). In the systems with 14 m long elements, this difference is equal to 82%. As expected and

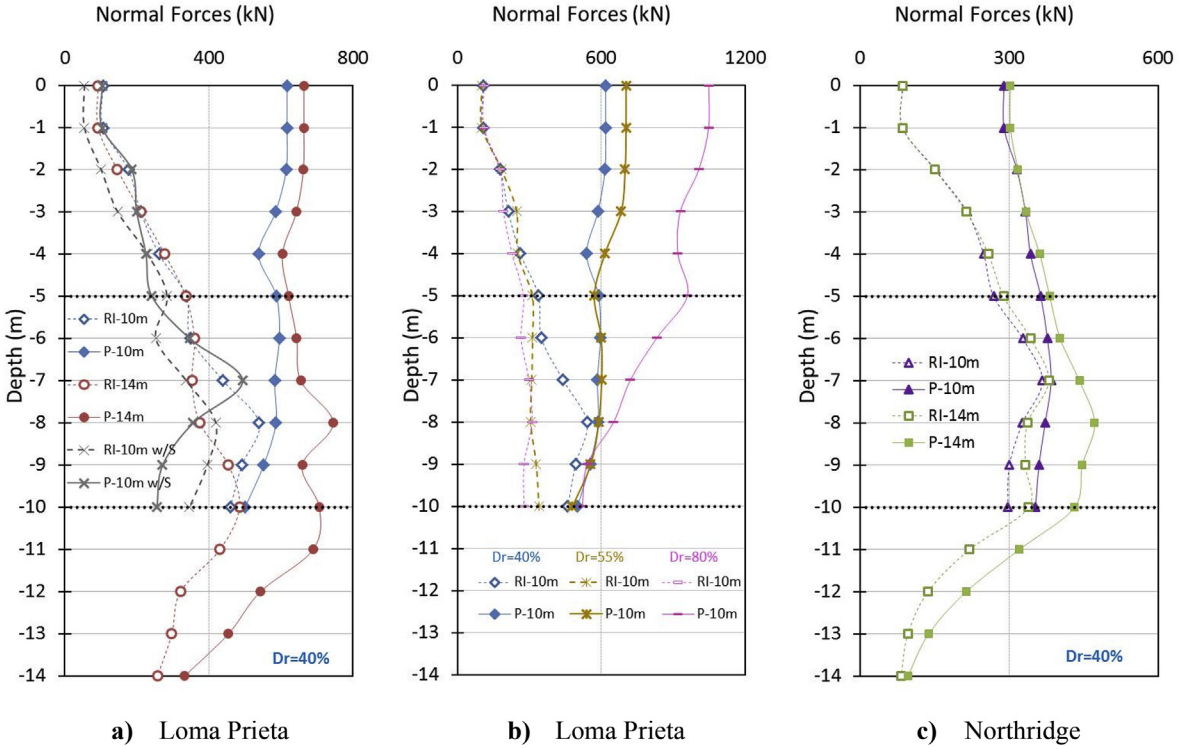

Fig. 12. Normal forces in rigid inclusion and pile systems for different conditions and earthquakes.

due to the inertial forces, in the systems without superstructure, the normal forces are also smaller.

The normal forces in the systems are increased with depth in the two shallowed layers and decreased in bedrock. It can be observed that a longer foundation element produces larger normal forces along the elements (Fig. 12a, c). The longer rigid elements absorb extra energy due to the higher contact surface with the surrounding soil principally when the liquefaction takes place. For instance, the moments in the system P-14 m are reduced in a range of 7%–26% compared to the P-10 m case (Fig. 12a). However, in the rigid inclusion cases, this range is smaller. Only at a 8 m depth, the difference is around 30%.

It can be noted that in the liquefiable soil with Dr = 40% under Loma Prieta earthquake, the values along the elements in the RI-10 m case are approximately 5%–42% smaller than the values in the P-10 m case while for the RI-14 m the forces are decreased 31%–52% respect to the P-14 m (Fig. 12a).

According to the shear forces developed in the superstructure, the normal forces in the pile cases are greater when the relative density of the liquefiable layer is augmented. For instance at 6 m depth, the moment of the P-10 m with Dr = 80% is reduced 28% respect to the systems with 55% and 40% relative density (Fig. 12b). This is contrary for the rigid inclusion cases in the liquefiable soil layer. The moment of the RI-10 m with Dr = 40% is increased 18% and 32% respect to the systems with Dr = 55% and Dr = 80%.

Similar as the bending moments, the normal forces are reduced in both pile and rigid inclusions as the input motion frequency increases (Fig. 12c). For example, the bending moments along the P-10 m with the Northridge earthquake are increased 36%–51% compare to the Loma Prieta earthquake. Similar behavior is displayed for the RI-14 m case where the increment is from 16% to 29%.

7.8. Displacements

Fig. 13 shows the horizontal displacements in the rigid elements. For all the cases with Dr = 40% and the Loma Prieta earthquake (Fig. 13a), the displacements are almost similar (0.18 m). This implies that the pile length and the consideration of superstructure have no influence on the level of displacements when the liquefaction is developed in the soil.

Fig. 13 (b) depicts the displacements for different relative densities. The maximum displacement in the pile head are 0.24 m and 0.18 m considering Dr = 80% and 40% respectively in the P-10 m case. It can be noted that the displacements decreases with depth in the rigid elements as stated by other authors [1,27].

In accordance with the previous results, the displacements in the pile and inclusion systems increased as the frequency of excitation is decreased (Fig. 13 c). A maximum displacement (0.08 m) of the rigid elements under the Northridge earthquake is obtained in the liquefiable layer. This implies a decrement of about 55% in the Loma Prieta earthquake case for systems with the same characteristics.

8. Conclusions

The effect of soil relative density, pile length, pile modelling type and earthquake predominant frequency on pile and rigid inclusion systems in liquefiable soil are examined. Three-dimensional analyses of these systems were developed. A 3-storey concrete building was considered in the study. The SANISAND constitutive model was used to represent the behavior of a liquefiable soil layer. This model is useful for different soil densities, stress levels and loading conditions. The analyses were carried out using dynamic coupled mechanical/groundwater simulations.

The response spectrum in all the analyzed case is reduced compared to the input motions due to the attenuation of energy in the liquefied soil layer. Linked to this result, the increment of the relative density in the sand layer implies greater accelerations at the ground surface. The response spectrum increases when the frequency of the excitation is decreased.

The superstructure shear forces using pile systems are greater than with rigid inclusion systems. These forces are also greater in the systems with longer rigid elements because they are subjected to inertial forces due to their embedded part in the bedrock, especially in liquefied soils.

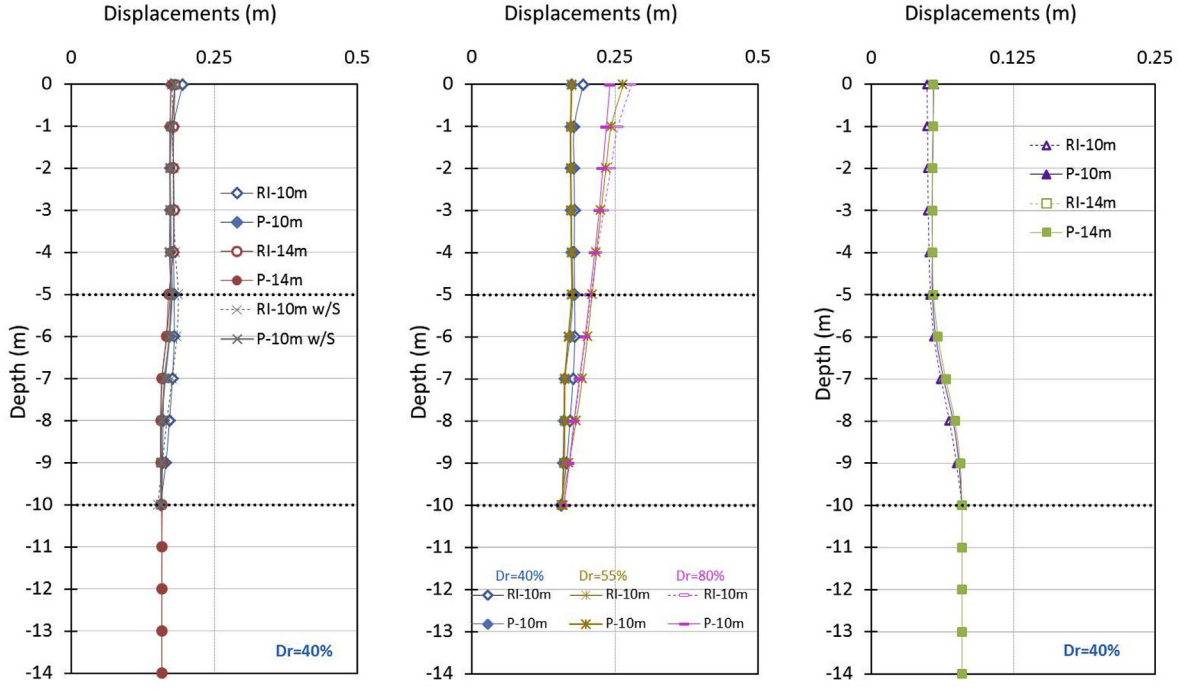

Fig. 13. Normal forces in rigid inclusion and pile systems for different conditions and earthquakes.

In accordance to the response spectrum, the shear forces are reduced as the relative density of the sand layer decreases, in the pile cases.

The increment in excess pore pressure ratio is more pronounced in the rigid inclusion cases than in pile cases. The excess pore pressure curves show important drops due to the excessive soil dilatation tendency of the SANISAND constitutive model. However, these pore pressure variations are reduced for the systems analyzed with the Northridge earthquake. The increment of the fundamental input motion frequency and relative density in the sand layer decrease the excess pore pressure ratio values. The consideration of the physical pile cross section increases the excess pore pressure values.

The maximum bending moments, normal forces and displacements in the rigid elements are increased with the increment of the sand layer relative density. However, they are reduced as the frequency of the earthquake increases. The maximum bending moments are located at the intersection of liquefiable and non-liquefiable soil layers. Longer rigid elements experiment greater normal forces due to the greater energy absorbed from the contact surface with the surrounding soil. Considering these results, further studies should be developed to investigate the influence of factors such as the position and the thickness of the liquefiable soil layer. It should be also interesting consider the influence of the variation of permeability during liquefaction in the considered systems.

Acknowledgement

This research is supported by the National Council of Science and Technology (CONACYT).

References

[1] Liyanapathirana DS, Poulos HG. Seismic lateral response of piles in liquefying soil. J Geotech Geoenviron Eng 2005;131:1466–79.
[2] Abdoun T, Dobry R, O'Rourke TD, Goh SH. Pile response to lateral spreads: centrifuge modeling. J Geotech Geoenviron Eng 2003;129:869–78.
[3] Abdoun T, Dobry R. Evaluation of pile foundation response to lateral spreading. Soil Dynam Earthq Eng 2002;22:1051–8.
[4] González L, Abdoun T, Dobry R. Effect of soil permeability on centrifuge modeling of pile response to lateral spreading. Journal of Geotechnical and Geoenviromental Engineering ASCE 2009;135(62):1.
[5] Ramirez J, Barrero A, Chen L, Dashti S, Ghofrani A, Taiebat M, et al. Site response in a layered liquefiable deposit: evaluation of different numerical tools and methodologies with centrifuge experimental results. J Geotech Geoenviron Eng 2018;144:4018073.
[6] Su D, Li XS. Effect of shaking intensity on seismic response of single-pile foundation in liquefiable soil. Ground modification and seismic mitigation vols. 97–102. GSP 152; 2006.
[7] Gao X, Ling XZ, Tang L, Xu PJ. Soil-pile-bridge structure interaction in liquefying ground using shake table testing. Soil Dynam Earthq Eng 2011;31:1009–17.
[8] Haeri SM, Kavand A, Rahmani I, Torabi H. Response of a group of piles to liquefaction-induced lateral spreading by large scale shake table testing. Soil Dynam Earthq Eng 2012;38:25–45.
[9] Tamura S, Tokimatsu K. Seismic earth pressure acting on embedded footing based on large-scale shaking table test. Geotechnical Special publication, **145**, ASCE, 2006. p. 83–96.
[10] Tokimatsu K, Suzuki H, Sato M. Effects of inertial and kinematic interaction on seismic behavior of pile with embedded foundation. Soil Dynam Earthq Eng 2005;25:753–62.
[11] Ashour M, Norris G. Lateral loaded pile response in liquefiable soil. J Geotech Geoenviron Eng 2003;129:404–14.
[12] Liyanapathirana DS, Poulos HG. Behaviour of pile groups in liquefying soil. GeoCongress 2006;2006:1–6.
[13] Phanikanth VS, Choudhury D, Reddy GR. Behavior of single pile in liquefied deposits during earthquakes. Int. J. Geomech. ASCE. 2013;13:454–62.
[14] Janalizadeh A, Zahmatkesh A. Lateral response of pile foundations in liquefiable soils. J. Rock Mech. Geotech. Eng. 2015;7:532–9.
[15] Maheshwari BK, Sarkar R. Seismic behavior of soil-pile-structure interaction in liquefiable soils: parametric study. Int. J. Geomech. ASCE 2011;11:335–47.
[16] Rahmani A, Pak A. Dynamic behavior of pile foundations under cyclic loading in liquefiable soils. Comput Geotech 2012;40:114–26.
[17] Wang R, Liu X, Zhang JM. Numerical analysis of the seismic inertial and kinematic effects on pile bending moment in liquefiable soils. Acta Geotech 2017;12:773–91.
[18] Wang R, Zhang JM, Wang G. A unified plasticity model for large post-liquefaction shear deformation of sand. Comput Geotech 2014;59:54–66.
[19] Beaty A, Byrne PM. An effective stress model for predicting liquefaction behavior of sand. Geotech. Eng. Soil Dyn. 1998;1:766–77.
[20] Boulanger R, Ziotopoulou K. Formulation of a sand plasticity model for earthquake engineering applications. Soil Dynam Earthq Eng 2013;53:254–67.
[21] Byrne PM. A cyclic sher volume coupling and pore-pressure model for sand. Second Int. Conf. Recent Adv. Geotech. Eng. Soil Dyn. 1991;1:47–55.
[22] Dafalias YF, Manzari MT. Simple plasticity sand model accounting for fabric change effects. J. Eng. Mech. ASCE. 2004;130:622–34.
[23] Tasiopoulou P, Gerolymos N. Constitutive modeling of sand: formulation of a new plasticity approach. Soil Dynam Earthq Eng 2016;82:205–21.
[24] Yang Z, Elgamal A, Parra E. Computational model for cyclic mobility and associated shear deformation. J Geotech Geoenviron Eng 2003;129:1119–27.
[25] Haldar S, Babu SGL. Failure mechanisms of pile foundations in liquefiable soil: parametric study. Int J Geomech 2010;10:74–84.
[26] Ren H, Lu X, Li P. Computer simulation on dynamic soil-pile-superstructure interaction system considering liquefiable foundation. 14th World Conf. Earthq. Eng. 2008.
[27] Choudhury D, Chatterjee K, Kumar A, Phule RR. Pile foundations during earthquakes in liquefiable soils – theory to practice 15SEE. 2014. p. 327–42.
[28] López Jiménez GA, Dias D, Jenck O. Effect of the soil–pile–structure interaction in seismic analysis: case of liquefiable soils. Acta Geotech 2018. https://doi.org/10.1007/s11440-018-0746-2.
[29] Taiebat M, Jeremić B, Dafalias YF, Kaynia AM, Cheng Z. Propagation of seismic waves through liquefied soils. Soil Dynam Earthq Eng 2010;30:236–57.
[30] Barrero AR, Taiebat M, Lizcano A. Application of an advanced constitutive model in nonlinear dynamic analysis of tailings dam. GEOQuebec 2015;2015:1–7.
[31] Cheng Z, Dafalias YF, Manzari MT. Application of SANISAND dafalias-manzari model in FLAC3D. Contin. Distinct Elem. Numer. Model. Geomech. 2013. 09-03:16.
[32] Rahmani A, Ghasemi Fare O, Pak A. Investigation of the influence of permeability coefficient on the numerical modeling of the liquefaction phenomenon. Sci Iran 2012;19:179–87.
[33] Shahir H, Pak A. Estimating liquefaction-induced settlement of shallow foundations by numerical approach. Comput Geotech 2010;37:267–79.
[34] Cheng Z, Jeremić B. Numerical modeling and simulation of pile in liquefiable soil. Soil Dynam Earthq Eng 2009;29:1405–16.
[35] Sadek M, Shahrour I. A three dimensional embedded beam element for reinforced geomaterials. Int J Numer Anal Methods Geomech 2004;28:931–46.
[36] Itasca F. 3D. Fast Lagrangian analysis of continya in 3-dimentions, version 5.0. The Manual 2012:1–108.
[37] Manzari MT, Dafalias YF. A critical state two-surface plasticity model for sands. Geotechnique 1997;47:255–72.
[38] Dafalias YF, Papadimitriou AG, Li XS. Sand plasticity model accounting for inherent fabric anisotropy. J Eng Mech 2004;130:1319–33.
[39] Taiebat M, Dafalias YF. SANISAND: simple anisotropic sand plasticity model. Int J Numer Anal Methods Geomech 2008;32(8):915–48.
[40] Li XS, DafaliasYF. Anisotropic critical state theory: role of fabric. J Eng Mech 2012;138:263–75.
[41] Li XS, Wang Y. Linear representation of steady-state line for sand. J Geotech Geoenviron Eng 1998;124:1215–7.
[42] Been K, Jefferies MG. A state parameter for sands. Geotechnique 1985;35:99–112.
[43] Arulmoli K, Muraleetharan KK, Hosain MM, Fruth LS. VELACS laboratory testinf program, soil data report. Technical report 90-0562. The Earth Technology Corporation. Irvine, CA: report to the National Science Foundation; 1992. https://doi.org/10.13140/2.1.3740.8320.
[44] Marti J, Cundall P. Mixed discretization procedure for accurate modelling of plastic collapse. Int J Numer Anal Methods Geomech 1982;6:129–39.
[45] Kuhlemeyer RL, Lysmer J. Finite element method accuracy for wave propagation problems. J. Soil Mech. Found. Div. ASCE. 1973;99:421–7.
[46] Okyay US. Sols renforcés par inclusions rigides: etude expérimentale et numérique des transferts de charge. Univ. Eur.; 2015. 10 6131566054.
[47] Lysmer J, Kuhlemeyer RL. Finite dynamic model for infinite media. J. Eng. Mech. Div. ASCE. 1969;95:859–78.
[48] Idriss IM, Lysmer J, Hwang R, Seed HB. QUAD-4 - a computer program for evaluating the seismic response of soil structures by variable damping finite element procedures Rep. EERC, Earthquake Engineering Research Center, University of California; 1973. 73/16:1-79.
[49] Suwal S, Pagliaroli A, Lanzo G. Comparative study of 1D codes for site response analyses. Int. J. Landslide Environ. 2014;2:24–31.
[50] Martin GR, Finn WDL, Seed HB. Funadmentals of liquefqction under cyclic loading. J Geotech Eng Div 1975;101:423–38.
[51] Hatem A. Comportement en zone sismique des inclusions rigides Analyse de l'interaction sol-inclusion-matelas de répartition-structure PhD thesis Lille, France: Université des Sciences et Technologies de Lille; 2009 [In French].
[52] Houda M. Comportement sous chargement cyclique des massifs de sol renforcés par inclusions rigides : expérimentation en laboratoire et modélisation numérique PhD thesis Université de Grenoble; 2016 [In French].
[53] Kumar A, Choudhury D, Katzenbach R. Effect of earthquake on combined pile – raft foundation. Int. Jounral Geomech. 2016;16(5):04016013–6.
[54] Mánica-Malcom MA, Ovando-Shelley E, Botero Jaramillo E. Numerical study of the seismic behavior of rigid inclusions in soft Mexico City clay. J Earthq Eng 2016;20:447–75.
[55] Alsaleh H, Shahrour I. Influence of plasticity on the seismic soil-micropiles-structure interaction. Soil Dynam Earthq Eng 2009;29:574–8.
[56] Kitiyodom P, Masumoto T, Kawaguchi K. Analyses of piled foundations subjected to ground movements induced by tunnelling. Geotechnical aspects of underground construction in soft ground 5th international symposium. IS Amsterdam; 2006. p. 551–7.
[57] Wotherspoon LM. Three dimensional pile finite element modelling using OpenSees.

NZSEE Conf. Proc. 2006;26:1–8.
[58] Banerjee S, Goh SH, Lee FH. Earthquake-induced bending moment in fixed-head piles in soft clay. Geotechnique 2014;64:431–46.
[59] Kourkoulis R, Gelagoti F, Anastasopoulos I, Gazetas G. Hybrid method for analysis and design of slope stabilizing piles. J Geotech Geoenviron Eng 2012;138.
[60] Montoya-Noguera S, Lopez-Caballero F. Effect of coupling excess pore pressure and deformation on nonlinear seismic soil response. Acta Geotech 2016;11:191–207.
[61] Popescu R, Prevost JH, Deodatis G, Chakrabortty P. Dynamics of nonlinear porous media with applications to soil liquefaction. Soil Dynam Earthq Eng 2006;26:648–65.
[62] Wang M, Chen G, Iai S. Seismic performances of dyke on liquefiable soils. J. Rock Mech. Geotech. Eng. 2013;5:294–305.
[63] Kramer S, Hartvigsen AJ, Sideras SS, Ozener PT. Site response modeling in liquefiable soil deposits. 4th IASPE/IAEE international symposium: effects of surface geology on seismic motion. 2011. p. 1–12.
[64] Koutsourelakis S, Prvost JH, Deodatis G. Risk assessment of an interacting structure-soil system due to liquefaction. Earthq Eng Struct Dyn 2002;31:851–79.
[65] Elgamal A, Yang Z, Parra E. Computational modeling of cyclic mobility and post liquefaction site response. Soil Dynam Earthq Eng 2002;22:259–71.
[66] Daftari A. New approach in prediction of soil liquefaction PhD Thesis Technische Universität Bergakademie Freiberg; 2015
[67] Ishihara K. Terzaghi oration : geotechnical aspects of the 1995 Kobe earthquake. Preceedings of ICSMFE. 1997. p. 2047–73.
[68] Finn WDL, Fujita N. Piles in liquefiable soils: seismic analysis and design issues. Soil Dynam Earthq Eng 2002;22:731–42.